Earthq Eng & Eng Vib (2020) 19: 649-668 **DOI**: https://doi.org/10.1007/s11803-020-0587-5

Novel uniaxial concrete constitutive model considering bond-slip effect

Liu Yongbin[1, 2†], Dai Junwu[1, 2‡], Yang Yongqiang[1, 2§] and Jiang Tao[1, 2†]

1. *Institute of Engineering Mechanics, China Earthquake Administration, Harbin 150080, China*

2. *Key Laboratory of Earthquake Engineering and Engineering Vibration, China Earthquake Administration, Harbin 150080, China*

Abstract: A uniaxial concrete constitutive model considering the bond-slip effect is proposed and its finite element analysis (FEA) implementation on a fiber section of a beam-column element is presented. The tension-stiffening, crack-closing, crack-opening, cyclic degradation of the tensile capacity of reinforced concrete are modeled, which reveals the significance of energy dissipation resulting from bond slip during crack opening and closing under cyclic loading. The model is based on a simplified mechanical concept in a smeared manner and verified through quasi-static test results of X-type slender RC columns. The FEA results using a common concrete model with no consideration of bond slip present significant pinching when predicting the hysteretic loop of slender columns, which is not consistent with the test results and underestimates the capacity of energy dissipation of cracking during cyclic load. The results obtained with the proposed model show good agreement with the test results, which can reflect the degradation of stiffness and strength as well as the energy dissipation of the crack opening and closing due to the bond slip effect. Considering its simplicity and computational efficiency, it is more applicable for analyzing large-scale structures than other methods that consider the bond-slip effect, especially for slender columns, such as those used in cooling towers and subjected to seismic excitation.

Keywords: bond slip; energy dissipation of cracking; reinforced concrete; slender column; fiber section; cyclic degradation

1 Introduction

The total lateral deformation of a reinforced concrete column is complex to simulate. It includes three components, namely, flexural deformation, shear deformation and bar slip after concrete cracking. To accurately predict the overall structural behavior, full consideration must be given to these deformation components. To better predict the cyclic response of reinforced concrete structures, many bond-slip models have been proposed. Eligehausen *et al*. (1983) published their early experimental work on the bond performance of reinforcing bars embedded in concrete blocks under monotonic and cyclic loadings, and proposed a bond stress-slip relationship. Figure 1 shows the bond resistance mechanism of a reinforcing bar embedded in concrete. It is assumed that the concrete is well-confined by hoops and splitting failure along the bar development length does not occur. Initially, the bond resistance is provided by the bearing of the ribs in a reinforcing bar. When concrete crushing occurs due to the rib bearing, the bond stress reaches its peak value (Fig. 1(a)). After peak strength, the bearing resistance significantly decreases, and residual bond strength is provided by the surface friction along the rib tips (Fig. 1(b)). Figure 1(c) shows the bond stress-slip relationship under load reversals. When the load reverses, the reinforcement bars slide in the opposite direction and the friction resistance is built up between the bar and the concrete until the crack surfaces come into contact. Under reversed-cyclic loading, the cracking and crushing of concrete lead to strength reduction, which cannot be recovered. After complete bearing failure of concrete ribs, the residual bond strength is developed by the friction mechanism and maintained uniformly, regardless of the slip deformation. Compared with the tension stiffening curve under monotonic loading, reversed cyclic loading reduces the bond strength and may lead to failure. The structural damage resulting from bond failure can be significant and determine global structural response.

The bond-slip relationship of concrete and reinforcement and the unrecoverable damage of the concrete around the ribbed rebar attributable to cyclic loading or plasticization of the rebar has been intensively investigated (Marti *et al*., 1998; Alvarez, 1998; International Federation for Structural Concrete (fib), 2013; Borosnyói and Balázs, 2005; Shima *et al*., 2011). For the uniaxial bond stress-slip relationships, a tension

Correspondence to: Dai Junwu, Institute of Engineering Mechanics, China Earthquake Administration, 29 Xuefu Road, Harbin 150080, China
Tel: +86-451-86652883
E-mail: junwudai@126.com
†PhD Candidate; ‡Professor; §Associate Professor

Supported by: National Key R&D Program of China under Grant No. 2018YFC1504404, Fund for Earthquake Engineering of China Earthquake Administration under Grant No. 201508023

Received November 17, 2018; **Accepted** April 25, 2019

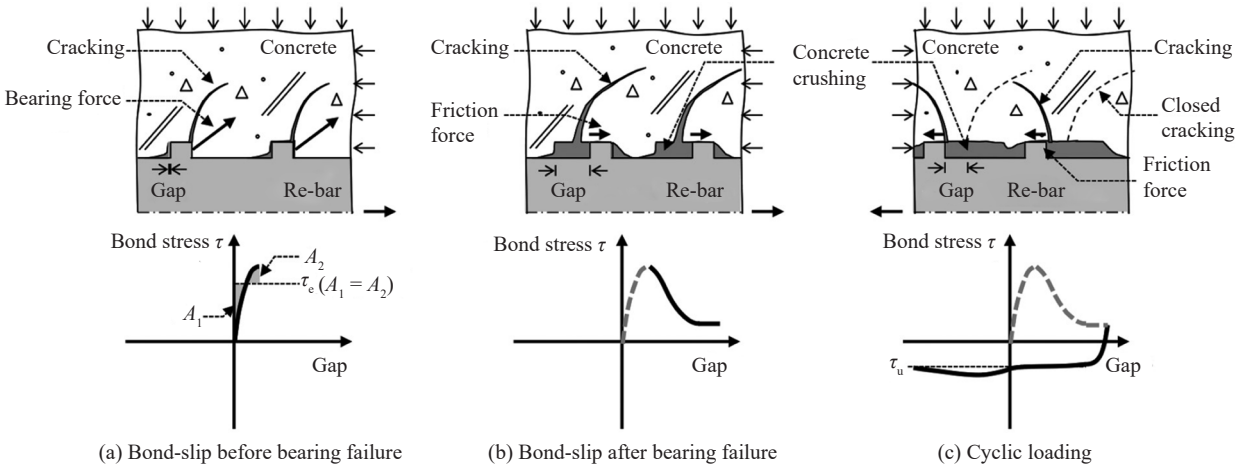

Fig. 1 Bond resistance mechanism of reinforcing bar (Hwang, 2015)

chord model (TCM) was proposed by Marti *et al*. (1998), on the basis of Rehm′s (1961) differential equation of slipping bond. The applications and developments of the TCM were carried out for a cracked membrane model by Kaufmann *et al*. (1998), loading cycles and fatigue of prestressed tension ties by Fürst (2001), investigations for bending based on fracture mechanics by Kenel (2002), and bending members under sustained loads by Burns (2011). Then the original TCM was modified to make it applicable to simulate the elastic and plastic states of the rebar under general unloading and reloading cycles by Koppitz *et al*. (2014).

A rebar embedded in concrete blocks subjected to tensile force will accumulate strain over its embedment length, which leads the rebar to extend or slip relative to the surrounding concrete blocks. In turn, the intact concrete between adjacent cracks has the capacity to carry tensile forces due to the interaction between concrete and reinforcement bar, bringing about a larger stiffness in comparison with the stiffness of the respective bare rebar, which is known as tension stiffening. Due to the tension stiffening effect, a load can be transferred from rebar to concrete via bond stress along the rebar surface between concrete cracks. In spite of the tensile strength of concrete accounting for a small amount of its compressive strength, it is important for the tension stiffening effect. Monti and Spacone (2000) proposed a new beam finite element explicitly accounting for the slip between the reinforcing bars and the surrounding concrete, whose formulation combines the fiber section model with the model of a reinforcing bar considering continuous bond-slip. Limkatanyu and Spacone (2003) developed two numerical models considering bond-slip effects, comprising a displacement-based RC frame element and a rigid beam-column joint element, which made the analytical results agree well with the test results in terms of strength, displacement demands and hysteretic energy dissipation. Lackner and Mang (2003) developed a one-dimensional composite model consisting of steel bars and the surrounding concrete introduced at the bar scale considering a nonlinear bond stress-bond slip relation. Lowes *et al*. (2004) successfully modeled the bond-slip effect of beam-column joints by applying a zero-length interface element between a two-dimensional concrete element and a steel truss element. Bentz (2005) proposed an expression to quantify the tension stiffening relationship based on a smeared crack approach.

For simulation of the bond-slip relationship, it is more accurate to use a distributed bond element, but it would make modeling much more difficult and the analyses process time-consuming. Therefore, a computationally efficient model that can consider the bond-slip effect is necessary to predict the overall structural response. Simplified total-strain-based membrane models that include bond-slip behavior have been developed for finite element analysis of RC members in Canada and the U.S. and applied to successfully analyze a variety of RC structures (So *et al*., 2009). A main advantage of the approach based on total strain is that the computing of crack widths and spacing can be avoided. Bond-slip behavior is considered indirectly according to tension stiffening relationships by calculating only the average stress and strain of the concrete and rebar. Membrane models based on total strain have been used successfully for analyzing a variety of concrete structures, such as the modified compression field theory (MCFT) (Palermo and Vecchio, 2007). When applying the membrane model based on total strain, either a fixed crack model (Mansour and Hsu, 2005) or a rotating crack model (Vecchio and Collins, 1986) has been adopted to construct the concrete constitutive model. So *et al*. (2009, 2010) developed a simplified, smeared total-strain-based model which divided a 2D membrane element into bonded and slip regions in the direction perpendicular to the orientation of the tensile cracks. The model was capable of simulating the bond-slip behavior under cyclic loading based on a simplified mechanistic concept

in an average manner. Kagermanov and Ceresa (2016) presented a physically based tensile model implemented in RC membrane elements, in which average concrete stresses of a cracked RC element were derived from equilibrium, compatibility, and constitutive relationships under biaxial cyclic loading conditions. The equations of the model governing tension stiffening as well as crack closing and opening explicitly accounted for cyclic bond degradation.

The motivation in this study is to simulate the nonlinear performance of slender columns, such as those used in the cooling towers, whose damage pattern is characterized by distributed flexural cracks extending from the ends to the middle as the horizontal deformation increases. As distributed bond elements are difficult to model and it is time-consuming to analyze large-scale structures, some 2D total strain based elements and constitutive models have been proposed considering the bond slip to simulate membrane elements. However, some features are not suitable for uniaxial materials. The software OpenSees provides a wide range of material models, elements, and solution algorithms to solve nonlinear problems and is open-source, which makes it convenient to develop new approaches according to the demand of research. Although it has provided several kinds of concrete constitutive models, such as Concrete01, Concrete02, Concrete04, Concrete06 and Concrete07, these models mainly focus on the constitutive model itself without bond-slip effect. Other uniaxial materials available related to the bond-slip effect are the BarSlip material and Bond_SP01 material. The BarSlip material is used to simulate the force versus slip response of a reinforcing bar which is anchored in a beam-column joint, and the Bond_SP01 material is used for capturing strain penetration effects at the column-to-footing, column-to-bridge bent caps, and wall-to-footing intersections. However, these two materials are not suitable to simulate the bond-slip effect on the distributed flexural cracks along the slender columns. Without consideration of the bond-slip effect, simulation cannot reflect the energy dissipation capacity due to the opening and closing of distributed flexural cracks in the slender columns. It also results in the disagreement of the simulation results with the test results of the force versus displacement of the slender columns, as observed in the analyses.

In order to solve this problem, a novel uniaxial constitutive model considering bond-slip effect was constructed to provide a simplified but reasonable method for use in the fiber section of a beam-column element to simulate RC columns under cyclic loading and is evaluated against quasi-static tests of two scaled slender column models of cooling towers. The proposed uniaxial concrete constitutive model can consider the tension-stiffening, energy dissipation due to crack opening and closing and the influence of concrete crushing on tension-stiffening. Compared with the concrete constitutive model proposed previously, some characteristics and parameters of the constitute model are modified, which is considered to be more reasonable.

2 Material constitutive models

Several nonlinear material models have been developed to simulate the force versus slip response of a rebar anchored in a beam-column joint or capture strain penetration effects at intersections such as the column to footing, wall to footing and column to bridge bent caps in the OpenSees framework; however, a uniaxial nonlinear material model for analyzing RC beams or columns considering the tensile and dissipation capacity of concrete crack opening and closing has not been made available through the OpenSees website. A proposed uniaxial reinforced concrete model considering bond-slip effect is discussed in the following subsections.

2.1 Uniaxial concrete model considering bond slip

2.1.1 Tensile regime

(1) Uncracked tensile response

The linear elastic response of concrete in tension is assumed up to its cracking strength f_{ct} and the tensile cracking strain ε_{ct} is calculated as

$$\varepsilon_{ct} = f_{ct} / E_c \tag{1}$$

where E_c is the initial elastic modulus of concrete.

(2) Tension-stiffening

The tension stiffening model simulates the phenomenon that, as a result of bond stress between rebar and concrete, a cracked concrete element can still withstand tension across cracks. Consequently, the effectiveness of rebar to transfer tensile forces across cracks needs to be determined in the tension stiffening models, which is primarily related to the material properties and geometry of the reinforcing bars across the cracks. A stepped bond stress is often assumed in an average way considering the bond-slip relationship. Sezen and Setzler (2008) proposed a macro-level approach treating the bond stress as a stepped function approximately, which predicts slip displacements reasonably well in comparison with five other commonly-used models found in the literature against three independent sets of test data. This model was also used for representing the effect of the slippage of the reinforcement bars inside the joints by Alva and Ana (2013) and for the simulation of anchorage slip in the footing by Pan *et al*. (2017). Zhang *et al*. (2016) presented an equivalent biuniform bond stress model obtained based on the equivalence of energy dissipation, to simplify the analytical model of bond stress between concrete and corroded steel rebar. The simplified model has an equivalent dissipated energy along the steel rebar length to the nonuniform distribution. The distribution of bond stress along the steel length is idealized as average

effective bond stress and frictional bond stress. The model provided a reasonable prediction for the flexural strength and failure modes of beams as shown by the results.

Marti *et al*. (1998) proposed a tension chord model (TCM) adopting a stepped, rigid-perfectly plastic relationship of bond shear stress versus slip. Although the relationship is a considerable simplification of the complex bond behavior, it provides reasonably accurate results compared with those from experiments. Based on the TCM, Koppitz *et al*. (2014) provided an analytical model to discuss the influence of bond degradation on the deformation behavior of a tension chord, which was successfully validated with experimental results. Studies herein refer to the results obtained by Marti *et al*. (1998) and Koppitz *et al*. (2014).

In the simple tension chord model (TCM) as previously discussed, problems of cracking, tension stiffening, minimum reinforcement and deformation capacity of concrete members are considered in a unified manner. Tensile forces are applied on an initially stress-free tension chord as shown in Fig. 2 (Marti *et al*., 1998; Alvarez, 1998). As stresses are produced by load, cracks are immediately fully developed. Constant average crack spacing S_{rm} occurs to all cracks as described by Eqs. (2) and (3)

$$S_{\mathrm{rm}} = \lambda S_{\mathrm{r0}} = \lambda \frac{\phi f_{\mathrm{ct}} (1-\rho)}{2\tau_{\mathrm{b0}} \rho} \tag{2}$$

$$0.5 \le \lambda \le 1.0 \tag{3}$$

where S_{r0} is the maximum crack spacing, ϕ is the diameter of the steel rebar, and $\rho = \frac{A_{\mathrm{s}}}{A_{\mathrm{c}}}$ is the geometrical reinforcement ratio. The constant λ can vary freely between the two boundaries of 0.5 and 1.0 in theory. In reality, however, λ is often determined by the spacing of the reinforcing bars. It was suggested (Marti *et al*., 1998) to assume the upper bond shear stress $\tau_{\mathrm{b0}} = 2 f_{\mathrm{ct}}$ for ordinary rebar, where is the tensile strength of concrete is the $0.3\left(f_{\mathrm{c}}^{'}\right)^{\frac{2}{3}}$ and f_{c}' is the cylinder compressive strength of concrete (in MPa).

When the concrete stress reaches its tensile strength, rebar stresses at the crack edge increase abruptly to crack stress σ_{sr0} to take over the tensile contribution of the concrete. Figures 2(b) and 2(c) show the two boundary crack patterns in Eq. (3) after they reach σ_{sr0}.

The entire global stress-strain path of a tension chord is illustrated in Fig. 3 under monotonic increasing load for both maximum and minimum crack spacing; steel strains $\varepsilon_{\mathrm{sm}}$ are averaged over the crack element and displayed on the abscissa. Whereas on the ordinate, steel stresses σ_{sr} are plotted. At the crack stress σ_{sr0} the $\varepsilon_{\mathrm{sm}}$ are reduced by a constant factor $\Delta\varepsilon_0$ compared with naked steel rebar, as presented in Eqs. (4) and (5).

$$\Delta\varepsilon = \frac{1}{4}\left(\frac{\sigma_{\mathrm{sr0}}}{E_{\mathrm{s}}} - \frac{f_{\mathrm{ct}}}{E_{\mathrm{c}}}\right) = \frac{f_{\mathrm{ct}}}{4E_{\mathrm{s}}}\frac{1-\rho}{\rho} \tag{4}$$

$$\Delta\varepsilon_0 = 2\lambda \times \Delta\varepsilon \tag{5}$$

As load increases further, the crack edge stress path follows a parallel line to the stress-strain relationship of the naked steel rebar at a distance of $\Delta\varepsilon_0$ until it reaches

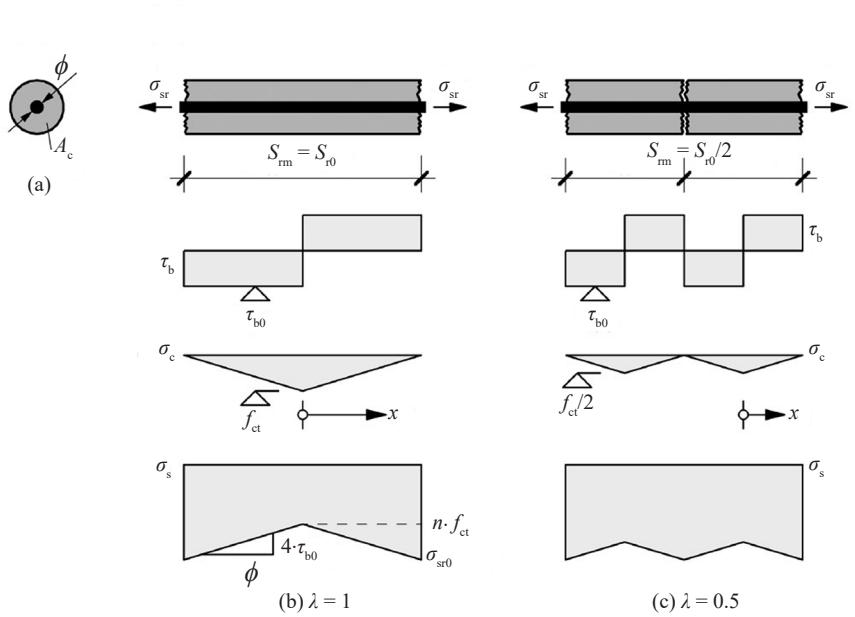

Fig. 2 (a) Tension chord with stress distributions at crack stress $\sigma_{sr} = \sigma_{sr0}$; (b) maximum crack spacing; (c) minimum crack spacing (Koppitz *et al*., 2014)

the yield strength f_{sy}.

Based on the mechanical concept above, the bond slip effect is considered in a smeared (average) manner for simplicity as shown in Fig. 4. Average concrete stresses are kept constant after the tensile strain exceeds ε_{ct} and equal to f_{ct} until arriving at the ultimate tensile strain ε_{ut} in the proposed model (see Fig. 5). According to Figs. 2–3 and Eqs. (2)–(5), ε_{ut} is the strain of the RC members when the crack formation phase is completed in the proposed model. Referring to CEB-FIP Model Code 1990 (CEB, 1993), the average crack spacing can be estimated as 2/3 S_{r0} . Accordingly, ε_{ut} is calculated as the strain when λ equals 2/3 (see Eq. (6)).

$$\varepsilon_{ut} = \varepsilon_{ct} + 8\Delta\varepsilon / 3 \tag{6}$$

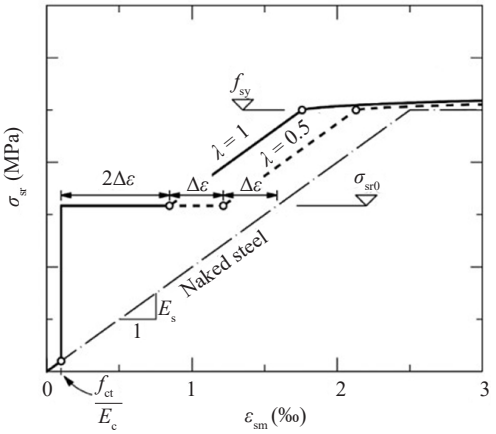

Fig. 3 Crack edge stress versus average steel strain relationship (Koppitz *et al*., 2014)

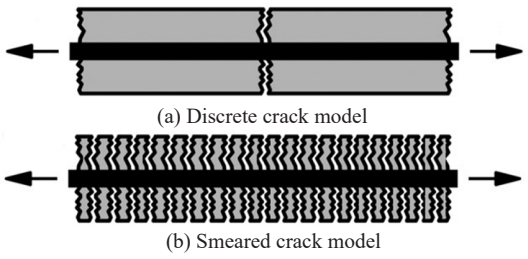

Fig. 4 One-dimensional illustration of smeared crack approach applied to reinforced concrete

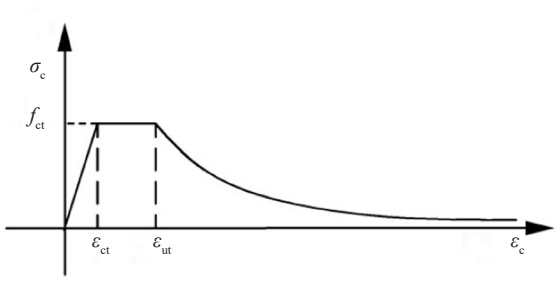

Fig. 5 Proposed tension stiffening model

When the concrete tensile strain exceeds ε_{ut}, the average tensile stress in the concrete reduces exponentially from f_{ct} to a limiting value of αf_{ct} at large tensile strains, according to the constitutive model proposed by Stevens *et al*. (1991). The parameter α is a function of the reinforcing ratio and distribution, which determines the frictional contact area and in turn affects the surrounding concrete behavior. Thus, for a concrete cross section containing n bars of diameter d_b, evenly distributed across its area A_c:

$$\alpha f_{ct} A_c = n\pi d_b \times Cf_{ct} \tag{7}$$

where $\alpha f_{ct} A_c$ is the total force transferred to concrete; $n\pi d_b$ is the area available for bond; and Cf_{ct} is the bond-stress parameter.

Assuming that the steel is evenly distributed

$$\rho = \frac{n\pi d_b^2}{4A_c} \tag{8}$$

Then

$$\alpha = C_t \frac{\rho}{d_b} \tag{9}$$

where $C_t = \frac{C}{4}$ is a constant having the units of length. It was found that a value of C_t is 75 mm provides acceptable agreement for a wide range of tests (Stevens *et al*., 1991).

According to Stevens *et al*. (1991), the equation for the proposed uniaxial concrete tensile response after cracking is

$$\frac{f_c}{f_{ct}} = (1-\alpha)\mathrm{e}^{-\lambda_f(\varepsilon_c - \varepsilon_{ut})} + \alpha \tag{10}$$

where ε_c and f_c are the strain and stress in the principal direction. Herein, the concrete tensile stress f_c is limited to the maximum stress that can be developed in the concrete due to friction between the steel and concrete. This friction stress approaches αf_{ct} in Eq. (10). The parameter λ_f controls the rate at which the response decays to the limiting value. It was proposed to make the parameter λ_f also a function of α .

$$\lambda_f = \frac{270}{\sqrt{\alpha}},\ \lambda_f \le 1000 \tag{11}$$

(3) Crack-closing and crack-opening

A crack-closing model represents the phenomenon when a cracked concrete element takes compression transferred from steel reinforcement indirectly due to bond-slip effect as the cracks are closed. Relatively stiff response for unloading from the tension stiffening curve is expected as presented in Fig. 6 when the load reverses

from the tension stiffening curve, because the friction has to be overcome before the reinforcement bars slide in the opposite direction. The friction to be overcome is assumed to be the same as the tension envelop value corresponding to the largest tension strain experienced (see Fig. 6).

Once the friction is overcome, the reinforcement bars slip in the opposite direction until the crack surfaces come into contact. Before fully closing of cracks under reversal load, compressive contact stresses will occur due to the misalignment between concrete crack surfaces and will increase after the concrete crack strain equals zero. To simulate this effect, cracks are assumed to be closed when the concrete strain reaches ε_{cl}. When the concrete compressive stress continues to increase and its strain is beyond ε_{cl} a transition curve is used to calculate the average concrete stresses, which will be introduced later. The strain of crack close ε_{cl} is calculated by Eq. (12).

$$\varepsilon_{cl} = \Delta\varepsilon_{cl} + \varepsilon_{i} \tag{12}$$

where $\Delta\varepsilon_{cl}$ is assumed to be 0.001, as referred to Kagermanov and Ceresa (2016), and ε_{i} is the strain of the intersection point of friction and the reloading path in the compression regime (Fig. 8).

Once reloading occurs in the process of unloading, the slope of the reloading path is the same as that of the unloading path, until the connection line between the point with the experienced maximum tensile strain and zero-load point with the residual strain ε_{re} is reached, and then load is applied along that connection line (see Fig. 7).

(4) Transition toward compressive strains

To simulate the effect that compressive stress increases from the contact of concrete crack faces to fully closing, average concrete stresses are directly determined from a transition curve connecting the crack-closing point (ε_{cl}, σ_{cl}) and the point of maximum experienced compressive strain on the monotonic envelope (ε_{cm}, σ_{cm}), which is shown in Fig. 8.

An *N*-power stress-strain relationship is used which provides a smooth transition between crack closing and compression reloading, referred to in Palermo and Vecchio (2003) and Kagermanov and Ceresa (2016), and given as

$$f_{c} = a + b\Delta\varepsilon_{c} + c\Delta\varepsilon_{c}^{N} \tag{13}$$

$$\Delta\varepsilon_{c} = \varepsilon_{cl} - \varepsilon_{c} \tag{14}$$

where *a, b, c* and *N* are parameters obtained such that the curve between the crack closing point (ε_{cl}, σ_{cl}) and the point (ε_{cm}, σ_{cm}).

The crack strain becomes zero at point (ε_{cl}, σ_{cl}) and thus, the concrete takes compression even though the average strain is positive. As the strain approaches zero, the concrete takes compression and continues reloading in compression. And the point (ε_{cm}, σ_{cm}) has the largest experienced compression strain on the monotonic compression envelope of concrete. These points should satisfy the tangent stiffness conditions below.

$$\sigma_{c}^{'}\left(\varepsilon_{cm}\right) = E_{cm} \tag{15}$$

$$\sigma_{c}^{'}\left(\varepsilon_{cl}\right) = E_{cl} \tag{16}$$

where $E_{cm} = E_{r}$ and $E_{cl} = 0$, and E_{r} is the reloading stiffness in the concrete compression regime, which will be discussed later.

(5) Influence of reversed cyclic loading

As compared to monotonic loading, reversed cyclic loading will reduce the bond strength, as shown in Fig. 9. According to the bond stress-slip relationship in "fib Model Code for Concrete Structures 2010", the values of the bond stress slip curve obtained from monotonic

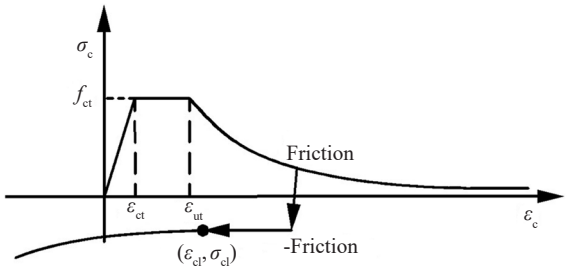

Fig. 6 Crack-closing model

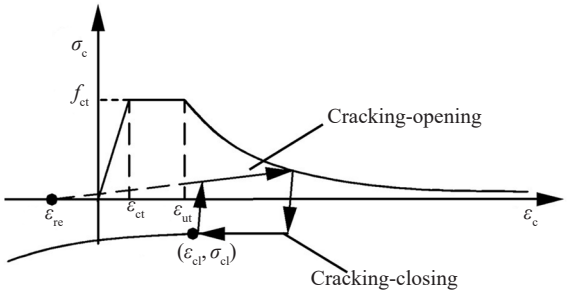

Fig. 7 Crack-opening model

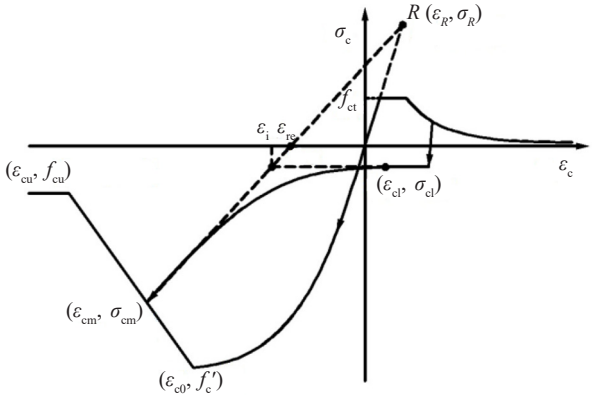

Fig. 8 Transition toward compressive strains

loading should be modified by the factor Ω_{cyc} in Eq. (17) based on the energy dissipation under cyclic loading, after the bond stress has reached its maximum value. Figure 9 also reveals the computing method of the dissipated energy under monotonic and cyclic loading (see the area under the monotonic and cyclic bond stress-slip curve, respectively).

$$\Omega_{cyc} = e^{\left[-1.2\left(\frac{\Lambda_{cyc}}{\Lambda_0}\right)^{1.1}\right]} \tag{17}$$

where Λ_{cyc} is the dissipated energy under cyclic loading, and Λ_0 is the dissipated energy under monotonic loading (Fig. 9).

For the proposed concrete model, a similar method based on the energy dissipation is used to consider the tensile capacity reduction due to reversed cyclic loading (see Fig. 10).

The dissipated energy under monotonic loading is the area under the tensile envelope curve from zero strain to the strain ε_3, which is the strain of the rebar when the slip reaches S_3. Herein, S_3 is obtained from Table 6.1-1 in the "fib Model Code for concrete structures 2010" and

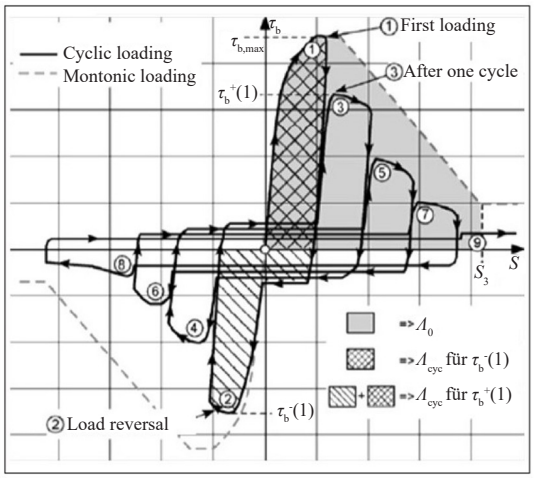

Fig. 9 Bond stress-slip relationship and definition of the dissipated energy under monotonic and cyclic loading (fib Model Code for Concrete Structures 2010)

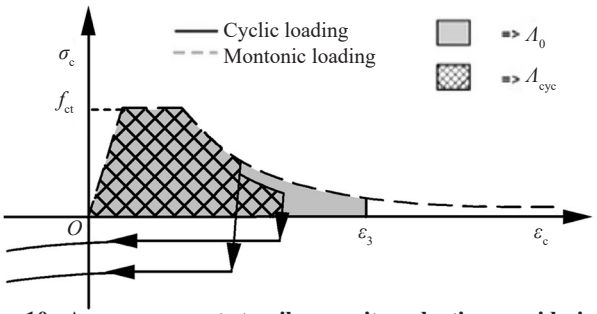

Fig. 10 Average concrete tensile capacity reduction considering bond slip effect under reversed cyclic loading

ε_3 is calculated as:

$$\varepsilon_3 = \frac{S_3}{l_b} \tag{18}$$

where l_b is the bond length which is given as 5ϕ, and ϕ is the diameter of the longitudinal rebar. The dissipated energy during cyclic loading is calculated as the cumulative energy dissipation under tension stress.

2.1.2 Compressive regime

For nonlinear finite element analysis of concrete in compression, many constitutive models have been proposed (ASCE, 1982; Ayoub and Filippou, 1998; Palermo and Vecchio, 2007). In these models, a constitutive model used in OpenSees (Mazzoni *et al*., 2006), Concrete02, provides acceptable accuracy and economical computational consumption. This model can simulate the stress-strain relationship of concrete under an arbitrary cyclic load. A detailed introduction of the model is presented in Mohd Yassin (1994). The model proposed herein is similar to that of Concrete02 in compressive regime, while the tensile regime is different. The compressive regime of the proposed model is described as follows.

(1) Loading and unloading

The envelope curve of concrete compression regime is defined by two key points: the peak point (ε_{c0}, f_c') and the crushing point (ε_{cu}, σ_{cu}). A quadratic compressive stress-strain relationship is assumed from the origin point up to the point (ε_{c0}, f_c') which is defined as (Scott *et al*., 1982)

$$\sigma_c = f_c'\left[2\left(\frac{\varepsilon_c}{\varepsilon_{c0}}\right) - \left(\frac{\varepsilon_c}{\varepsilon_{c0}}\right)^2\right],\ 0 < \varepsilon_c \le \varepsilon_{c0} \tag{19}$$

where σ_c and ε_c are the concrete stress and strain; f_c' is the concrete strength; and ε_{c0} is the strain corresponding to f_c'.

As the compressive strain increases, the capacity envelop will degrade linearly defined by a straight line (Eq. (20)) between the two key points. After the compressive strain beyond the crushing point (ε_{cu}, σ_{cu}), the compressive capacity will keep the value σ_{cu} constant (Eq. (21)).

$$\sigma_c = f_c' + \frac{\sigma_{cu} - f_c'}{\varepsilon_{cu} - \varepsilon_{c0}}\left(\varepsilon_c - \varepsilon_{c0}\right),\ \varepsilon_{c0} < \varepsilon_c \le \varepsilon_{cu} \tag{20}$$

$$\sigma_c = \sigma_{cu},\ \varepsilon_c > \varepsilon_{cu} \tag{21}$$

As the experienced minimum strain ε_{cm} decreases, a successive stiffness degradation occurs in the hysteretic behavior of unloading and reloading. It is described by a set of straight lines (see Fig. 11). The stiffness degradation is determined by letting all the unloading

curves converge to a common Point R as shown in Fig. 11. The strain and stress at Point R (ε_R, σ_R) are calculated as

$$\varepsilon_R = \frac{\sigma_{cu} - d_{cu} E_c \varepsilon_{cu}}{E_c (1 - d_{cu})} \tag{22}$$

$$\sigma_R = E_c \varepsilon_R \tag{23}$$

where d_{cu} is a damage parameter defined as the ratio between the unloading slope at the crushing point (ε_{cu}, σ_{cu}) and the initial slope E_c.

The residual strain ε_{re} is obtained from the residual strain point, which is the intersection of the line between the unloading point and Point R and the horizontal strain axis. The slope of the line between the unloading point and Point R is the damage stiffness, denoted as E_r. Therefore, the instantaneous reloading stiffness in the compression region is given as

$$E_r = \frac{\sigma_R - \sigma_{cm}}{\varepsilon_R - \varepsilon_{cm}} \tag{24}$$

where ε_{cm} is the minimum strain that the current model has ever experienced and σ_{cm} is the stress corresponding to ε_{cm} obtained from the concrete compressive envelop.

The unloading and reloading lines (see Fig. 11) do not coincide but form a triangular loop. The unload stiffness is the initial stiffness E_c at first, and then it will unload by the slope of $0.5E_r$ after unloading to a straight line passing through the residual strain point whose slope is $0.5E_r$. Once reloading occurs in the process of unloading, the slope of the reloading path is the initial stiffness E_c until the connection line between the unloading point and the R point is reached, and then load is applied according to the damage stiffness E_r (see Fig. 11).

(2) Transition toward tensile strains

Tension stiffening and tensile capacity reduction due to reversed cyclic loading after initial cracking are considered in the tensile behavior model, as previously mentioned. As shown in Fig. 12, the tensile stress can appear anywhere along the strain axis. For example, tensile stress can occur under a tensile strain due to initial cracking, and can also occur under a compressive strain resulting from reloading after an unloading from a compressive state.

In Fig. 12, assuming Point N is the current zero-load crossing point from compression to tension and Point L has the experienced maximum tensile strain, a straight line connecting Points N and L is adopted to determine the reloading curve. Thus, the strain and stress of Point L (ε_L, σ_L) are calculated as

$$\varepsilon_L = \varepsilon_{re} + \varepsilon_{max} \tag{25}$$

where ε_{max} is the experienced maximum strain difference between the tensile strain and zero-load crossing point. And σ_L is the stress on the concrete tensile envelope line whose tensile strain is ε_{max}.

(3) Influence of crushing on tension stiffening

To consider the influence of compression crushing on the tensile bond slip, the concrete tensile capacity will drop to zero once the concrete compression strain reaches the crushing strain ε_{cu}, which is shown later in Figs. 15 and 16.

2.1.3 Comparison between concrete models with and without consideration of bond-slip effect

The proposed model considering bond-slip effect, referred to as ConcreteBS, is compared with the model Concrete02 commonly used in OpenSees. Figure 13 shows the difference between the monotonic envelopes of the two models.

To compare the two uniaxial models under cyclic load, two different cyclic strain loads are applied, as shown in Fig. 14, which impose tension first and compression first, respectively. Taking as an example, the parameters are defined as f_c' = -44.67 MPa, ε_{c0}= -0.0026, σ_{cu}= -8.9 MPa, ε_{cu}= -0.0034, f_{ct} = 3.78 MPa, the geometrical reinforcement ratio is 0.02 and the diameter of the longitudinal bars is 8 mm.

The difference between the two models under cyclic loading of tension first and compression first is shown in Figs. 15 and 16, respectively. It is obvious that

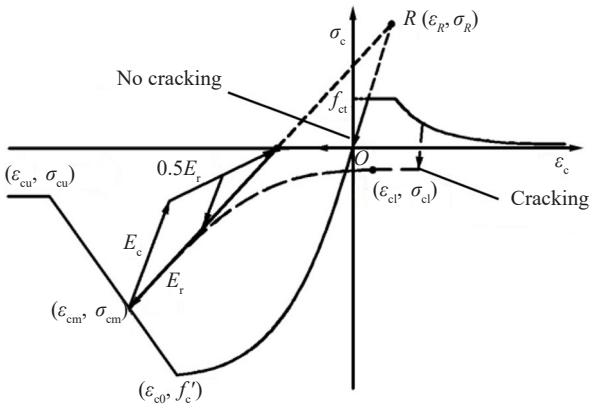

Fig. 11 Hysteretic rule of the proposed concrete model

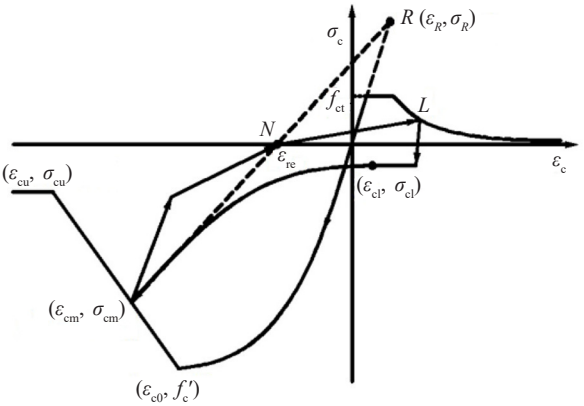

Fig. 12 Transition regime from compression to tension

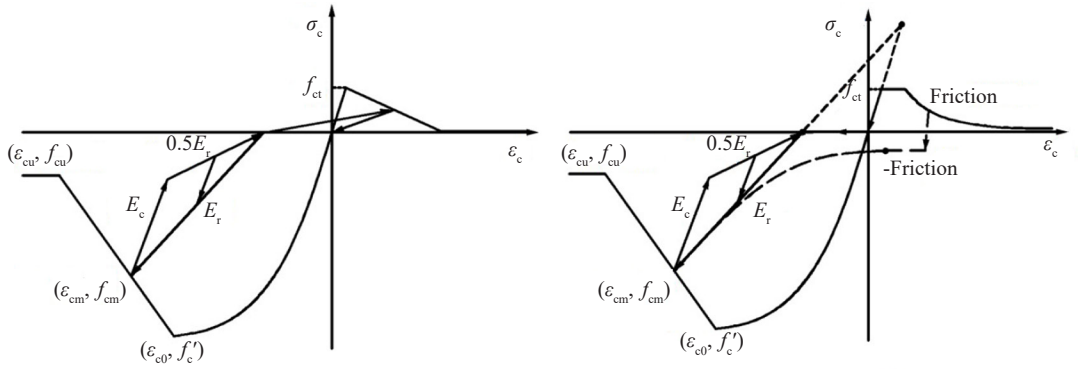

(a) Concrete02 (b) ConcreteBS

Fig. 13 Comparison of monotonic envelope between Concrete02 and ConcreteBS

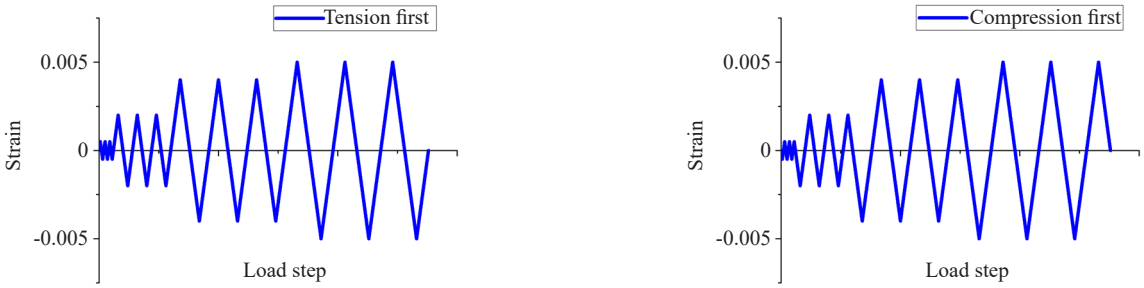

(a) Tension first (b) Compression first

Fig. 14 Strain load of tension first and compression first

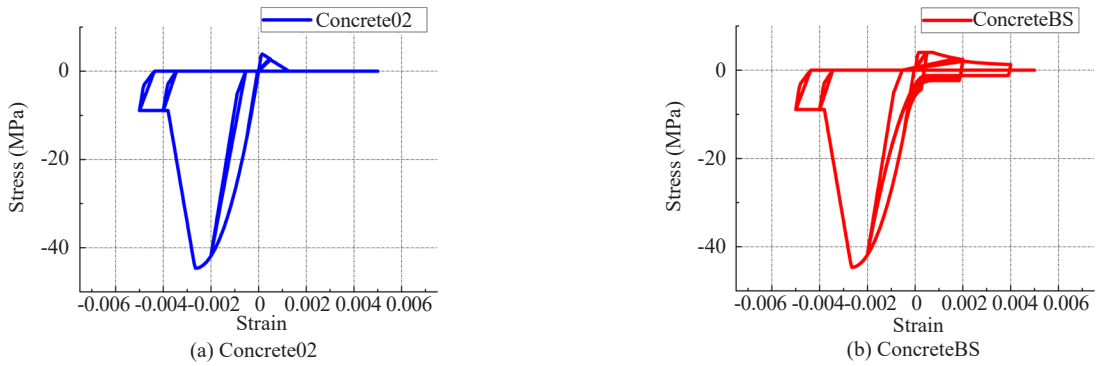

(a) Concrete02 (b) ConcreteBS

Fig. 15 Comparison of Concrete02 and ConcreteBS under cyclic loading (tension first)

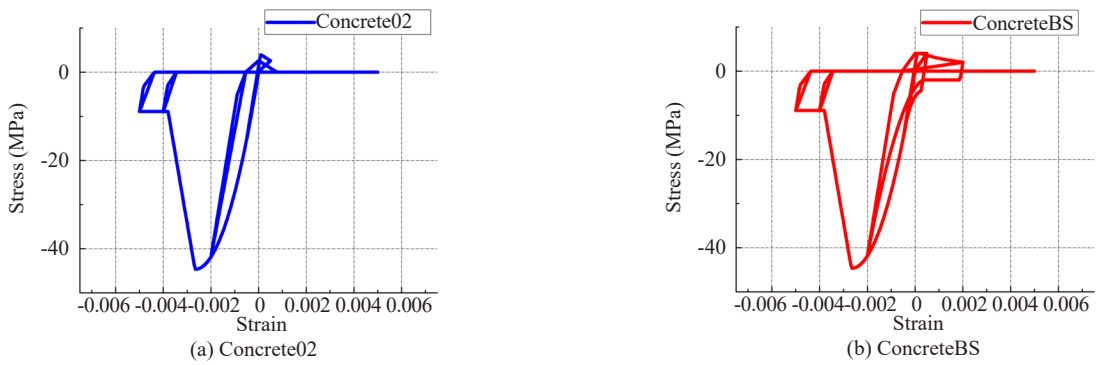

(a) Concrete02 (b) ConcreteBS

Fig. 16 Comparison of Concrete02 and ConcreteBS under cyclic loading (compression first)

Concrete02 does not consider the friction and energy dissipation due to crack closing and opening, while the proposed model ConcreteBS can consider the energy dissipation during crack opening and closing resulting from the bond-slip effect.

2.2 Uniaxial steel model considering bond-slip effect

Many reinforcing steel models presenting the classical reinforcing steel behavior have been developed and are available. Steel models proposed by Seckin (1981) and Yokoo and Nakamura (1977) have been used in implementing total strain-based membrane models such as MCFT and Cyclic Softening Membrane Model (Mansour and Hsu, 2005), respectively. Hoehler and Stanton′s steel model (2006) was used for the previous bond slip membrane model study (So *et al*., 2009). Average steel stresses are determined by adopting a uniaxial model for a mild steel bar embedded in concrete.

To ensure that the total stress of concrete and steel rebar cannot exceed the yield stress of the steel rebar when the concrete reaches the tensile strength, a method of simply reducing the yield stress of the bare bar is used herein. As the simulation of steel rebar adopts uniaxial material, the strain-hardening stage of the reinforcing bar can still be simulated, but with its yield strength reduced. Because the reduction value of yielding stress is much smaller than the value of its yielding stress, the reduction has little effect on the strain-hardening stage of the steel rebar. After the concrete cracks occur, the average concrete tensile capacity will degrade and the steel rebar stress will increase beyond its yield strength and enter the strain-hardening stage. A similar method has been used by Stevens *et al*. (1991) to propose a constitutive model for the analysis of 2D reinforced concrete structural elements, which showed no loss of accuracy by working strictly in terms of average strains and stress for both the concrete and the reinforcing steel. So *et al*. (2009, 2010) adopted a method that the uniaxial envelope curve of bare steel was reduced by a factor related to the amount of average concrete frictional stress, to propose an RC material model that included frictional bond-slip behavior for use in a 2D total strain-based finite element analysis, which was validated with cyclic panel test results and RC shear wall experimental results. Kagermanov and Ceresa (2016) presented a physically based tensile model for RC membrane elements subjected to cyclic loading conditions, by using the same simplified method to account for the simulation of steel rebar. This model was implemented within a fixed-crack membrane finite element and verified against experimental tests on shear panels and RC walls. The analyses of RC walls with coupled flexure-shear behavior showed relatively good agreement with the overall lateral force-displacement response. Permanent displacements, stiffness degradation, hysteretic pinching and calculated crack patterns were in reasonable agreement.

In theory, the total stress, namely the sum of the average concrete and steel stresses at an open crack, cannot exceed the yield stress and therefore, the bare steel stress used for fiber beam-column elements must be reduced to represent the average steel stress. A simple method to achieve this is to reduce the yield envelope of the bare bar according to the limiting amount of concrete tension resulting from the groups of bars in question. The average yield stress $f_{\mathrm{y}}^{\mathrm{av}}$ of the embedded bar is determined according to Belarbi and Hsu (1994)

$$f_{\mathrm{y}}^{\mathrm{av}} = (0.91 - 2B) f_{\mathrm{y}} \tag{26}$$

$$B = \frac{1}{\rho}\left(\frac{f_{\mathrm{ct}}}{f_{\mathrm{y}}}\right)^{1.5} \tag{27}$$

3 Verification

3.1 Quasi-static tests of slender columns

Two RC column models in the shape of an X used in cooling towers were selected to verify the analysis capability of the proposed material model. Quasi-static tests were conducted on the two columns with the top fastened to a four bar linkage mechanism (see Fig. 20) to restrain the rotation, in order to simulate the boundary condition in the real cooling tower. The dimensions of the column model are shown in Fig. 17.

The two column specimens, referred to as S1 and S2,

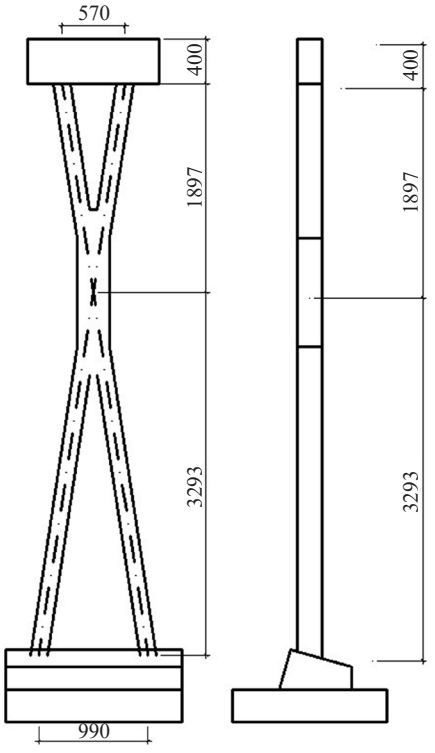

Fig. 17 Dimension of the column model (mm)

have different kinds of reinforcement arrangements. The rebar in the middle section of S1 is continuous, while that of S2 is discontinuous, as shown in Fig. 18.

Figure 19 illustrates the reinforcement details for S1 and S2. C45 Class concrete is used and its compressive strength f_c' is 44.67 MPa in tests. The longitudinal bars are HRB400 steel bar with a diameter of 8 mm. Their yielding strength is 476.4 MPa and their ultimate strength is 620.4 MPa. The stirrups adopt ribbed bars with the diameter of 6 mm. Their yielding strength is 333.8 MPa and their ultimate strength is 468.2 MPa.

The loading schematic is shown in Fig. 20.

The columns are loaded under two compression levels of 424 kN and 848 kN in the vertical direction, which correspond to the dead load and the maximum combined design load, respectively. The load ratio corresponding to a vertical load of 424 kN is 0.14, and that corresponding to a vertical load of 848 kN is 0.28. The transversus load is applied at the top of the column in the direction perpendicular to the plane of the column and controlled by displacement. The amplitude level of the displacement is 5 mm, 10 mm, 15 mm, 20 mm, 30 mm, 40 mm, 50 mm, 75 mm, 100 mm and 150 mm, respectively, and each level undergoes three cycles. The drift ratio corresponding to 150 mm is 1/35. Figure 21 provides the loading system of the quasi-static tests of the two specimens S1 and S2, and Fig. 22 shows the loading in the process of the test.

The strains of the reinforcement bars were monitored in the tests. The strain gauges of the steel bars were placed in four different elevations of the column models; namely the top, middle-upper, middle-lower and bottom (see Fig. 23). At the elevation of each single column, the strains of four steel bars at the corner were monitored. There are 32 strain monitoring points, referred to as P1–P32. P1–P8 are placed at the top, P9–P16 at the middle-upper elevation, P17–P24 at the middle-lower elevation and P25–P32 at the bottom of the column model.

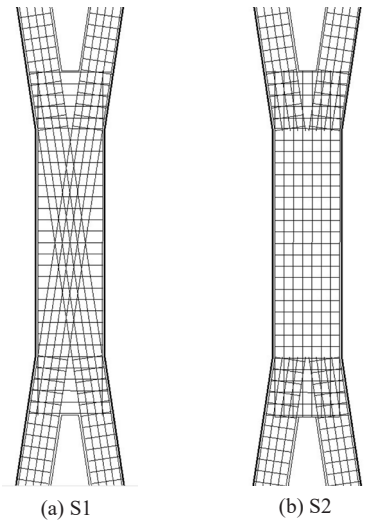

(a) S1 (b) S2

Fig. 18 Reinforcement arrangement of the middle sections

In order to obtain the global force-displacement of columns, the reaction force and displacement of the loading point are also monitored, including that of the horizontal actuator and the vertical actuator.

Based on the monitored global force-displacement of loading points, the hysteretic loops and skeleton curves of top displacement and reaction force in the transversus direction are shown in Fig. 24 (under vertical compression of 424 kN) and Fig. 25 (under vertical compression of 848 kN). The skeleton curve comparison of S1 and S2 in vertical compression of 424 kN and 848 kN is shown in Fig. 26.

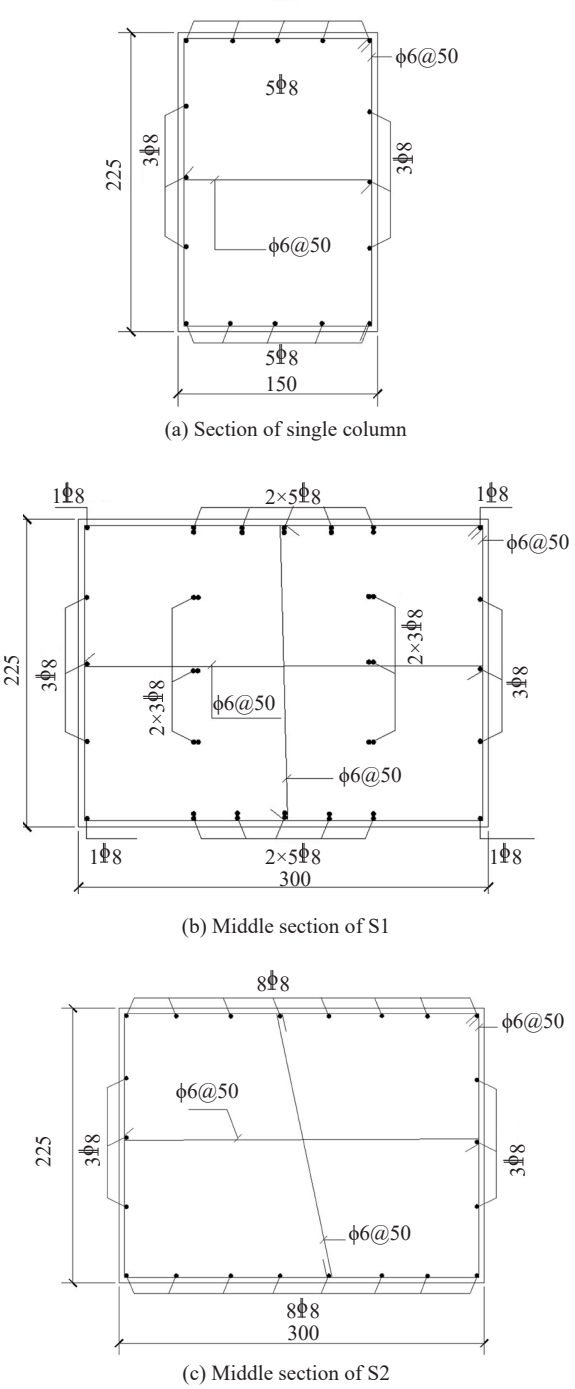

Fig. 19 Reinforcement details

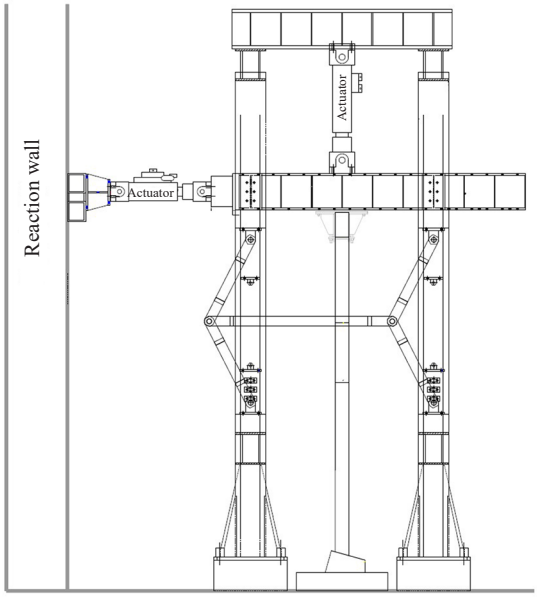

Fig. 20 Loading schematic

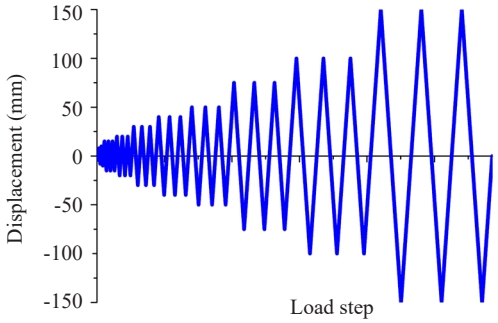

Fig. 21 Loading system

Fig. 22 Quasi-static test

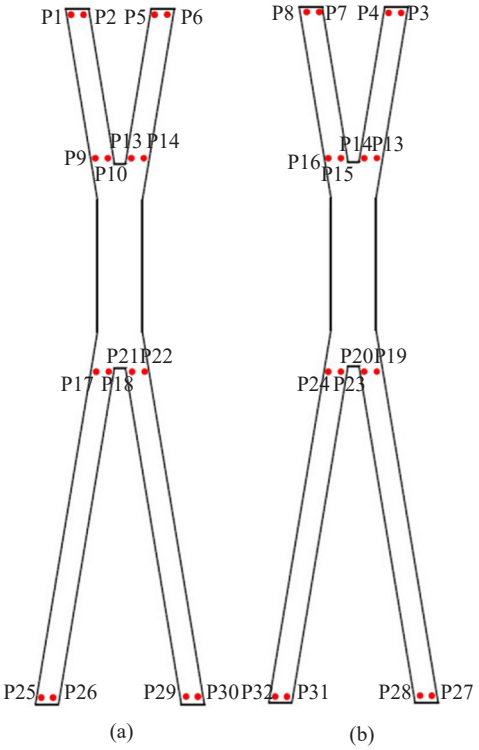

Fig. 23 Strain monitoring points of steel bars: (a) front view and (b) back view

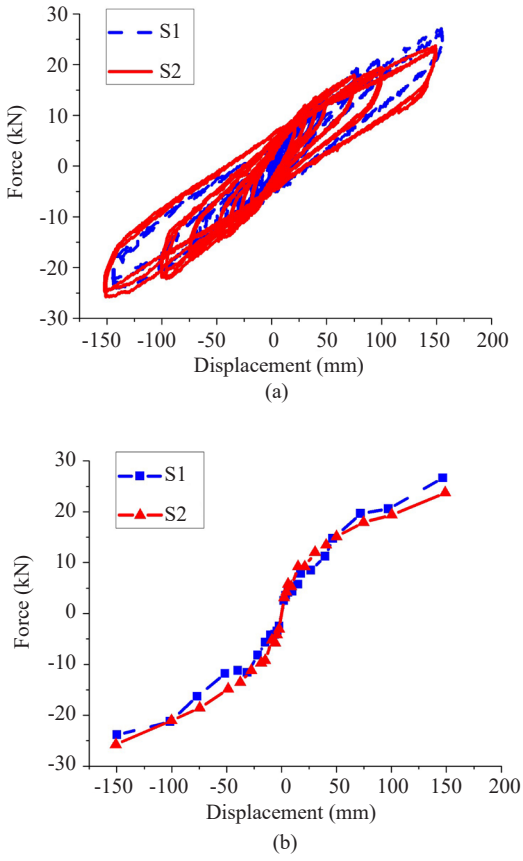

Fig. 24 Capacity comparison under the compression of 424 kN : (a) hysteretic loops and (b) skeleton curves

The comparison of the hysteretic loops above reveals that there is no significant difference in the flexural capacity between S1 and S2 when the vertical compression of 424 kN is loaded. Resulting from the second-order effect, the flexural capacity degradation of both S1 and S2 occurs when that of 848 kN is loaded. However, the flexural capacity of S2 degrades more seriously than S1. Due to the second-order effect, flexural capacity of the columns in the vertical compression of 848 kN is lower than that of 424 kN. It was observed that as larger loading displacement in the horizontal direction was applied, the reduction of flexural bearing capacity was more significant, as shown in Fig. 26.

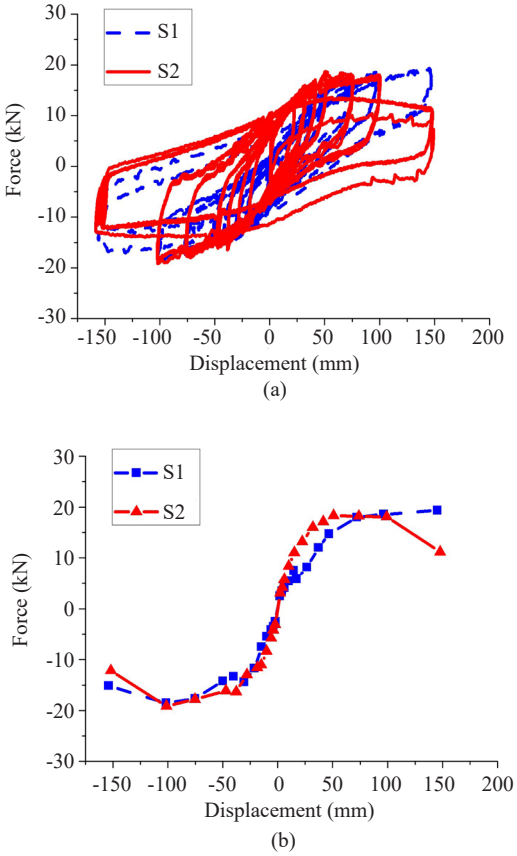

Fig. 25 Capacity comparison under the compression of 848 kN : (a) hysteretic loops and (b) skeleton curves

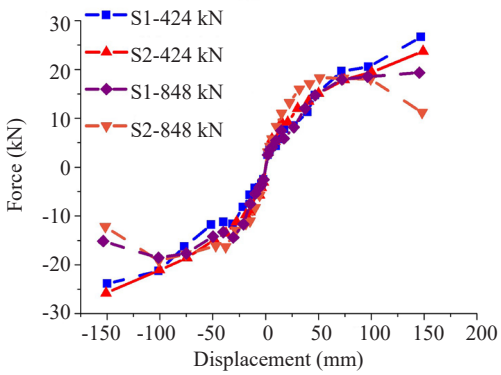

Fig. 26 Comparison of skeleton curves

The monitored strains of 32 bars were compared. The relation curves between strain and loading displacement in each load case is presented, and the strain amplitude is also compared between S1 and S2. The strain amplitude ε_A in each load case is calculated as

$$\varepsilon_A = \frac{|\varepsilon_+ - \varepsilon_-|}{2} \tag{28}$$

where ε_+ and ε_- are the strains corresponding to the maximum and minimum displacements in the positive and negative direction, respectively.

Due to space limitations, only the strains of bars in the measured points at the top and bottom of the column are presented, as shown in Figs. 27 and 28.

As is well known, the curvature ϕ of the column can be calculated as

$$\phi = \frac{2\varepsilon_s}{L} \tag{29}$$

where ε_s is the bar strain under bending moments only, not including the strain resulting from axial load, and L is the space between the monitored rebars in the direction

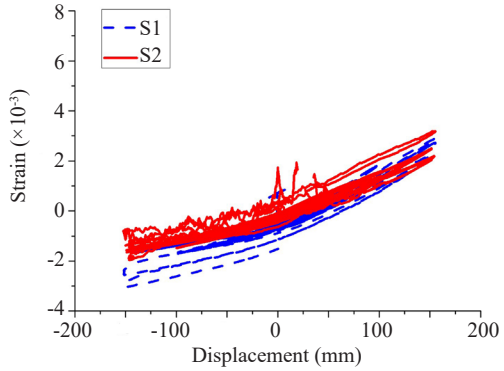

Fig. 27 Comparison of rebar strain of P6

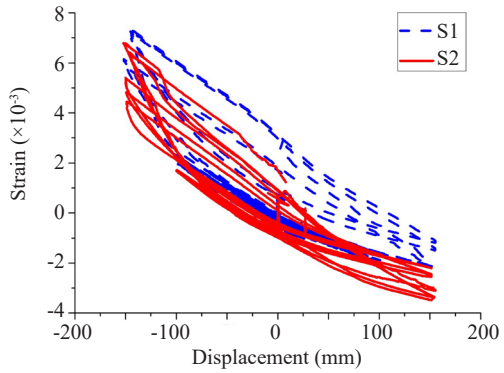

Fig. 28 Comparison of rebar strain of P29

of displacement loading, as shown in Fig. 29. Because the strain amplitude is calculated as Eq. (28), the strain was deducted due to axial load. For the slender columns in the cooling tower, flexural deformation is the main reason leading to its drift under wind load or earthquake action, so the strain amplitude can be used to calculate the curvature.

The average curvature of the column section, ϕ_{ave}, in the same elevation of strain monitoring points is calculated as

$$\phi_{ave} = \frac{2\varepsilon_{ave}}{L} \tag{30}$$

where ε_{ave} is the average strain amplitude at the same elevation. The average curvature of the column in each elevation of monitoring points in each load case is shown in Fig. 30.

From the comparison results of the steel rebar strain amplitude and curvature between S1 and S2 in each load case, no significant difference is found as the displacement amplitude increases. The curvature at the top of S1 increases slightly more obviously and shows nonlinearity in the load case with the displacement of 150 mm, which is also confirmed with the observation of its local concrete cover crushed.

The progression of damage (shown in Fig. 31) is similar for both specimens, which reveals that transversus flexural cracking extends from both ends of the columns to the middle as the top deformation amplitude of the columns increases. During the cyclic displacement load, the crack opening and closing is obvious, and the flexural crack is distributed along the entire column (Fig. 32).

The damage pattern and crack distribution details at the top, middle and bottom of the two columns are shown in Figs. 33–35, respectively. Different from common columns, no obvious compressive concrete crushing was observed and no concentrated hinge was formed, even under the displacement loading with a drift ratio of 1/35 in the tests.

Figure 36 shows the macroscopic crack-opening of the bottom of a column when the top of the column

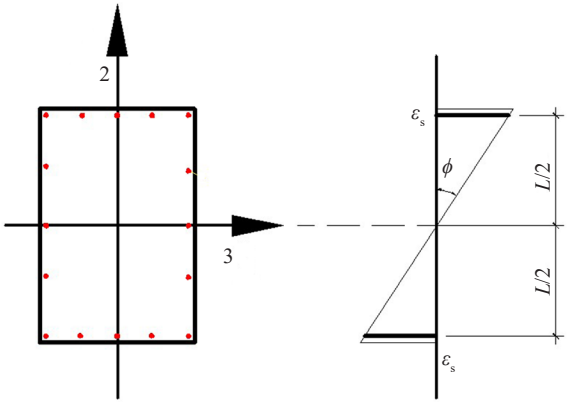

Fig. 29 Relation between ϕ and the steel rebar strain ε_s

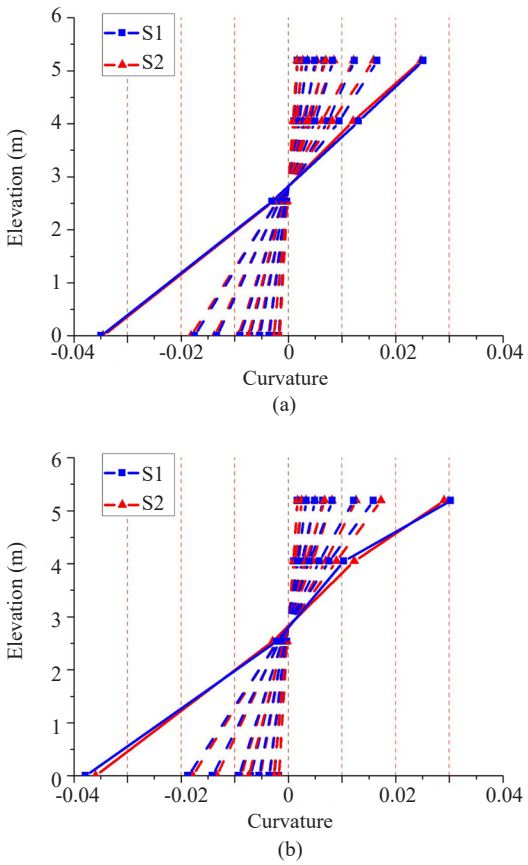

Fig. 30 Comparison of curvature: (a) under the compression of 424 kN and (b) under the compression of 848 kN

Fig. 31 Damage of the two specimens

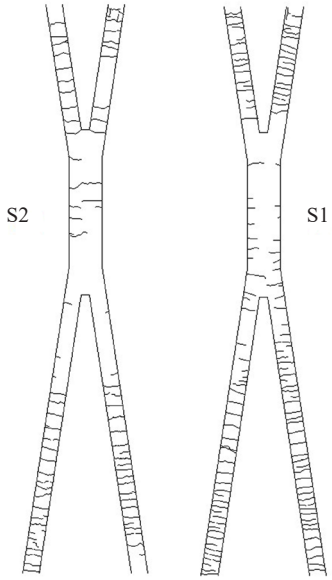

Fig. 32 Crack distribution

Fig. 33 Damage of the top of columns

Fig. 34 Damage of the middle of columns

Fig. 35 Damage of the bottom of columns

was undergoing large deformation in the test, which is obvious because the crack width is too large.

3.2 Finite element analysis using the proposed model

For slender RC columns under large horizontal deformation, the damage pattern is characterized by distributed flexural cracks extending from the ends to the middle, as observed in the tests of X-type columns. It is different from the common columns, whose damage is characterized by concentrated plastic hinge at the ends. The deformation and energy dissipation of common columns mainly results from the concentrated plastic hinges, while the bond-slip effect of flexural cracks is insignificant. Consequently, even if the bond-slip effect for the common columns is neglected, the simulation results of force versus displacement may agree with the test results to some extent. However, for slender columns, the opening and closing of distributed flexural cracks has obvious effect on the relationship of force versus deformation and energy dissipation capacity. If it is neglected in the simulation, the relationship of force versus deformation cannot be accurately predicted.

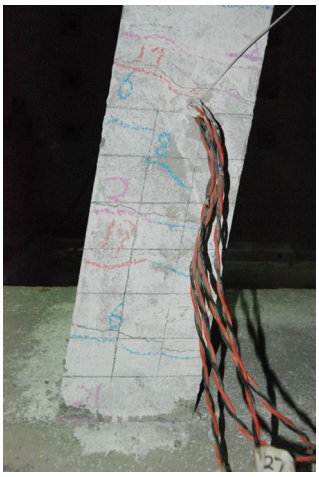

(a) One side of the bottom of a column

(b) The other side of the bottom of a column

Fig. 36 Cracking of the bottom of a column

In view of the discussion above, two different material models, referred to as Model NS (no slip) and Model BS (bond slip), are used in the fiber section. Model NS simply adopts an existing uniaxial concrete model Concrete02 in the platform of OpenSees, while Model BS adopts the proposed concrete model considering the bond-slip effect. As the uniaxial model Concrete02 in OpenSees is commonly used, the proposed model ConcreteBS has a similar compressive regime but a different tensile regime when compared with Concrete02. Consequently, the simulation results adopting the proposed model were compared with those adopting Concrete02. For both models, a uniaxial Giuffre-Menegotto-Pinto steel material object with isotropic strain hardening, referred to as Steel02 in OpenSees (Filippou *et al*., 1983), is used in this study. A displacement-based beam-column element with a fiber section is used to simulate the two slender columns.

To determine the effective concrete area in tension, referred to as $A_{c,ef}$, where the bond-slip effect is necessary to be considered, Fig. 37 is referred to according to the fib Model Code for concrete structures 2010. In Fig. 37, x is height of the compression zone; $Ø$ is the diameter of the anchored bar considered A_s is the gross reinforcement area in the effective concrete area in tension; $\rho_{s,ef}$ is the effective reinforcement ratio, calculated as $\frac{A_s}{A_{c,ef}}$.

In the simulation of columns in the tests, the confined and non-confined concrete were simulated using the same model as shown in Eq. (19) and Eq. (20), but with different parameters in the analyses. The difference is that, due to the confinement effect of stirrups, the compressive strength and corresponding strain of confined concrete is higher than that of the non-confined concrete, which is calculated according to the recommended model by Chang and Mander (1994).

According to the distribution of effective concrete area in tension and the area confined by stirrups, the section of X-type columns is divided into three areas, referred to as Area I, Area II and Area III, as shown in Fig. 38. Area I is the concrete cover, which is simulated using the model ConcreteBS to consider the bond-slip effect but no confinement effect; Area II belongs to not only the effective tension area but also the confinement area, which is simulated using the model ConcreteBS considering the confinement effect of stirrups; Area III is simulated using the model Concrete02, considering the confinement effect only.

In the effective concrete area in tension, due to the difference of reinforcement distribution, a different effective reinforcement ratio is used as shown in Fig. 39. The effective reinforcement ratio in the area enclosed by red lines is $\rho_{s1,ef}$, and that enclosed by blue lines is $\rho_{s2,ef}$.

In the analysis case of X-type columns in the tests, according to the distribution of confined concrete, for the fiber section definition of Area I in Fig. 38, the f_c' = -44.67 MPa, ε_{c0} = -0.00267 MPa, σ_{cu} = -8.9 MPa, ε_{cu} = -0.008 , f_{ct} = 3.78 MPa; for the definition of the confined section Area II and Area III, f_c' = -53.47 MPa, ε_{c0}=-0.00578, σ_{cu}=-30.99 MPa, ε_{cu}=-0.017, f_{ct}=3.78 MPa, obtained from the recommended model by Chang and Mander (1994). According to the distribution of effective concrete in tension as shown in Fig. 39, $\rho_{s1,ef}$= 0.107 and $\rho_{s2,ef}$= 0.034.

Adopting the simulation method above, a comparison of the global force-displacement response of the two slender columns between the FEA analyses and the tests was conducted. Figure 40 shows the cyclic results of the simulation using materials Model NS and Model BS, respectively, in comparison with test results of S1 under the vertical compression of 424 kN. Figure 41 is the comparative results of S1 under the vertical compression

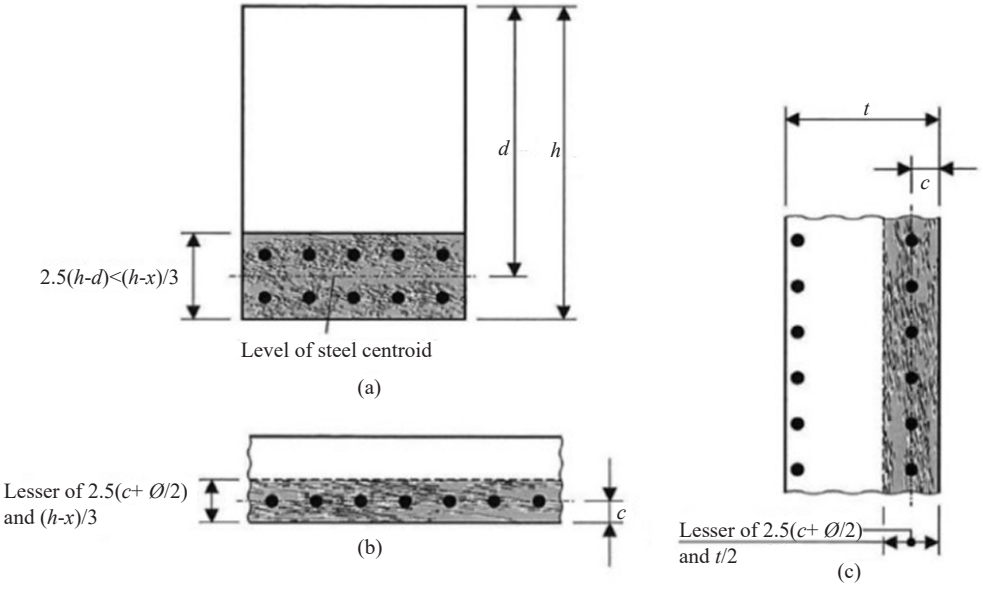

Fig. 37 Effective tension area of concrete for: (a) beam; (b) slab; (c) wall in tension (shaded areas, fib Model Code 2010)

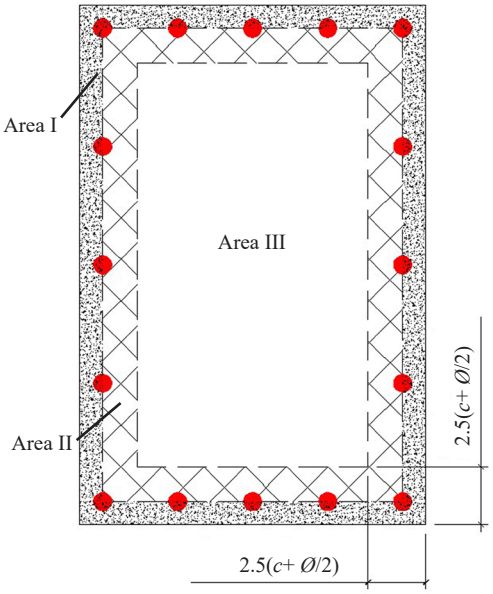

Fig. 38 Division of the column cross section

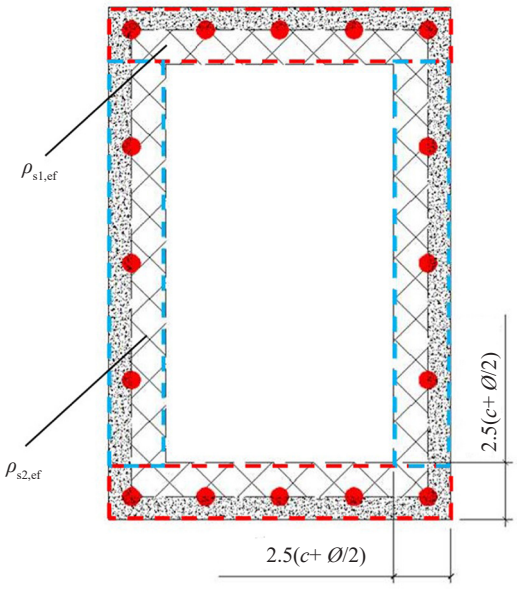

Fig. 39 Section division according to the effective reinforcement ratio

of 848 kN. Figures 42 and 43 are the similar comparative results of S2.

In comparison with the experimental results (Figs. 40–43), the proposed Model BS yields much better force-displacement response than Model NS. Model NS presents significant pinch phenomenon, which disagrees with the test results. Model BS using the proposed concrete constitutive model considering bond-slip effect shows good agreement with the hysteretic loops, which can reflect the bond-slip influence on the degradation of stiffness and strength and especially the energy dissipation of crack opening and closing under

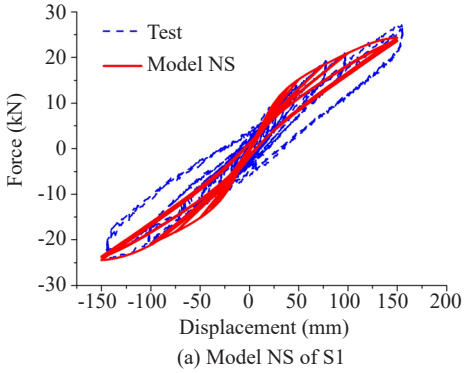

(a) Model NS of S1

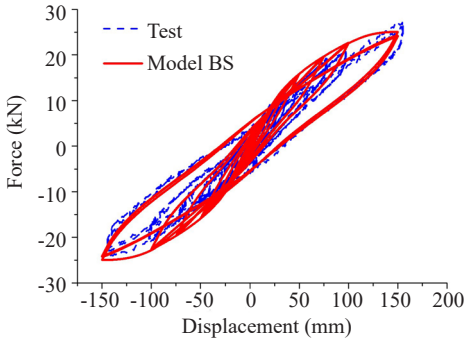

(b) Model BS of S1

Fig. 40 Comparison of Model NS and Model BS with test results of S1 (compression 424 kN)

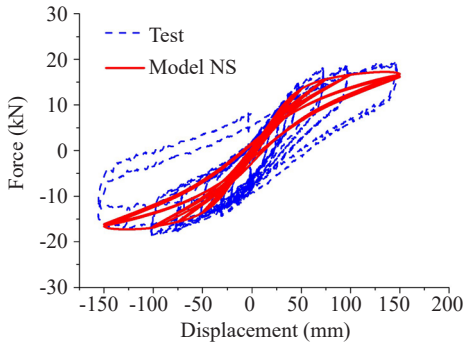

(a) Model NS of S1

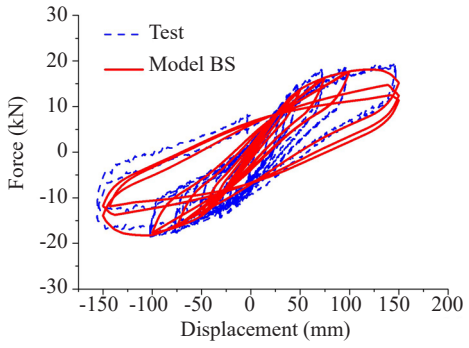

(b) Model BS of S1

Fig. 41 Comparison of Model NS and Model BS with test results of S1 (compression 848 kN)

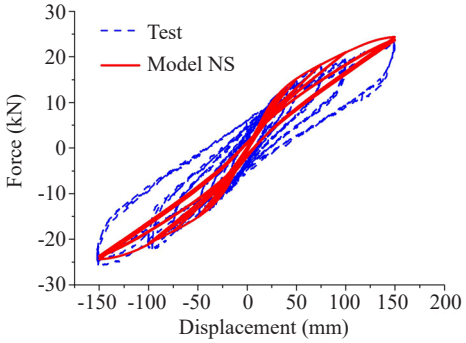

(a) Model NS of S2

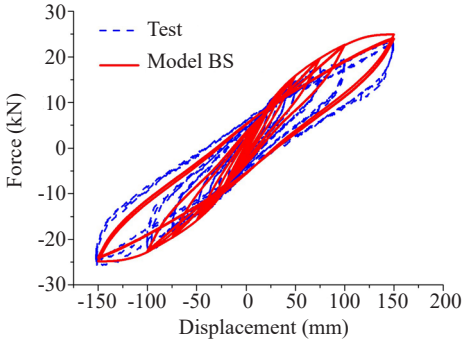

(b) Model BS of S2

Fig. 42 Comparison of Model NS and Model BS with test results of S2 (compression 424 kN)

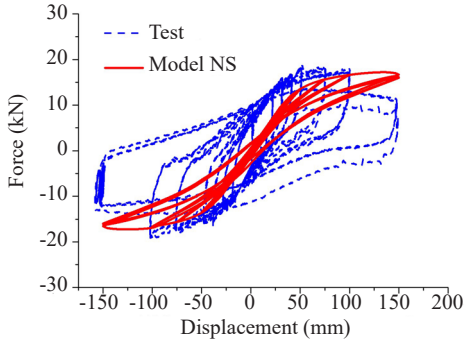

(a) Model NS of S2

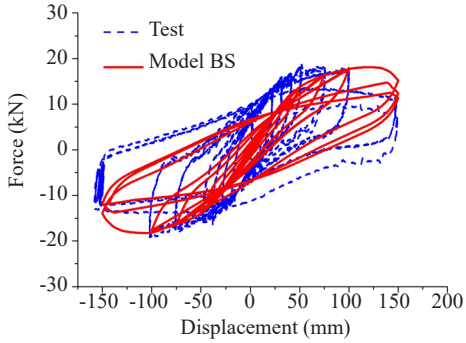

(b) Model BS of S2

Fig. 43 Comparison of Model NS and Model BS with test results of S2 (compression 848 kN)

cyclic loading. It is evident that the proposed model is applicable and efficient particularly for the nonlinear analyses of slender columns, whose damage pattern are characterized by flexural crack under cyclic loading, such as those of the cooling towers under seismic excitation.

4 Conclusions

A novel uniaxial concrete constitutive model considering the bond-slip effect is proposed, and an integrated experimental and finite element analyses are presented.

(1) Based on a simplified mechanical concept in a smeared manner, the proposed model includes the tension-stiffening, crack-closing, crack-opening, cyclic degradation of tensile capacity, which reveals the significance of energy dissipation during crack opening and closing under cyclic loading. In contrast with models that consider bond slip proposed by others, the characteristics of loading and unloading and their parameters are modified according to previous analyses and tests, which is considered to be more reasonable.

(2) To verify the proposed constitutive model considering bond slip, quasi-static tests of two slender column models of X shape used in cooling towers were conducted. Under the cyclic load on the top of the columns controlled by displacement perpendicular to the plane of columns in the shape of X, the progression of damage is similar for both specimens. Transversus flexural cracking extending from both ends of the columns to the middle appear as the top deformation amplitude of the columns increased. During the cyclic displacement load, the crack opening and closing were observed, and the transversus crack is distributed along the entire columns.

(3) Compared with the common concrete model, the proposed model predicts the hysteretic loop of this kind of slender column reasonably well. The FEA results using a common concrete model without consideration of bond slip shows significant pinch, which disagrees with the test results and underestimates the capacity of energy dissipation after cracking during cyclic load. The results of the proposed model can reflect the degradation of stiffness and strength and the energy dissipation of the crack opening and closing due to the bond slip effect. It is suitable for finite element analysis applied in the fiber section of the beam-column element. Due to its simplicity and computational efficiency, it is more applicable to analyze large-scale structures than other methods considering bond-slip effect, especially for slender columns, such as those used in cooling towers and subjected to seismic excitation.

References

Alva GMS and El Debs Ana Lúcia Homce de Cresce (2013), "Moment-rotation Relationship of RC Beam-Column Connections: Experimental Tests and Analytical Model," *Engineering Structures*, **56**: 1427–1438.

Alvarez M (1998), "Einfluss des Verbundverhaltens auf das Verformungsvermögen von Stahlbeton," *Doctoral Thesis*, ETH Zürich, Switzerland. (in Germany)

ASCE (1982), "State-of-the-art Report on Finite Element Analysis of Reinforced Concrete," *Report*, ASCE, New York.

Ayoub A and Filippou FC (1998), "Nonlinear Finite-Element Analysis of RC Shear Panels and Walls," *Journal of Structural Engineering*, **124**(3): 298–308.

Belarbi A and Hsu TTC (1994), "Constitutive Laws of Concrete in Tension and Reinforcing Bars Stiffened by Concrete," *ACI Structural Journal*, **91**(4): 465–474.

Bentz EC (2005), "Explaining the Riddle of Tension Stiffening Models of Shear Panel Experiments," *Journal of Structural Engineering*, *ASCE*, **131**(9): 1422–1425.

Borosnyói A and Balázs GL (2005), "Models for Flexural Cracking in Concrete: The State of the Art," *Structural Concrete*, **6**(2): 53–62.

Burns C (2011), "Serviceability Analysis of Reinforced Concrete Based on the Tension Chord Model," *Doctoral thesis*, ETH Zürich, Switzerland.

CEB (Comite´ Euro-International du Be´ton) (1993), *CEB-FIP Model Code 1990: Model Code for Concrete Structures*, Thomas Telford, London.

Chang GA and Mander JB (1994), "Seismic Energy Based Fatigue Damage Analysis of Bridge Columns: Part 1 - Evaluation of Seismic Capacity," *Technical Report*, NCEER-94-0006.

Eligehausen R, Popov EP and Bertero VV (1983), "Local Bond Stress-Slip Relationships of Deformed Bars under Generalized Excitations," *Report UCB/EERC-83/23*, EERC, University of California, Berkeley, CA, 169 pp.

fib (2013), *fib Model Code for Concrete Structures 2010*, fib Journal Structural Concrete, Ernst & Sohn, Berlin, Germany, 157.

Filippou FC, Popov EP, Bertero VV (1983), "Effects of Bond Deterioration on Hysteretic Behavior of Reinforced Concrete Joints," *Report EERC 83-19*, Earthquake Engineering Research Center, University of California, Berkeley.

Fürst, A. (2001), "Vorgespannte Betonzugglieder im Brückenbau," *Doctoral Thesis*, ETH Zürich, Switzerland. (in Germany)

Hwang HJ, Eom TS and Park HG (2015), "Bond-Slip Relationship of Beam Flexural Bars in Interior Beam-Column Joints," *ACI Structural Journal*, **112**(6): 827–837.

Hoehler MS and Stanton JF (2006), "Simple Phenomenological Model for Reinforced Steel under Arbitrary Load," *Journal of Structural Engineering*, **132**(7): 1061–1069.

Kagermanov A and Ceresa P (2016), "Physically Based Cyclic Tensile Model for RC Membrane Elements," *Journal of Structural Engineering*, **142**(12): 04016118.

Kaufmann W (1998), "Strength and Deformations of Structural Concrete Subjected to In-Plane Shear and Normal Forces," *Doctoral Thesis*, ETH Zürich, Switzerland.

Kenel A (2002), "Biegetragverhalten und Mindestbewehrung von Stahlbetonbauteilen," *Doctoral Thesis*, ETH Zürich, Switzerland. (in Germany)

Koppitz R, Kenel A and Keller T (2014), "Tension Chord Model Modification for Uniaxial Unloading and Reloading in Elastic and Plastic States," *Journal of Structural Engineering*, **140**: 04014077.

Lackner R and Mang HA (2003), "Scale Transition in Steel-Concrete Interaction. Part I: Model," *Journal of Engineering Mechanics*, **4**(393): 393–402.

Limkatanyu S and Spacone E (2003), "Effects of Reinforcement Slippage on the Non-Linear Response under Cyclic Loadings of RC Frame Structures," *Earthquake Engineering and Structural Dynamics*, **32**(15): 2407–2424.

Lowes LN, Moehle JP and Govindjee S (2004), "Concrete-Steel Bond Model for Use in Finite Element Modeling of Reinforced Concrete Structures," *ACI Structural Journal*, **101**(4): 501–511.

Mansour M and Hsu TTC (2005), "Behavior of Reinforced Concrete Elements under Cyclic Shear. II: Theoretical Model," *Journal of Structural Engineering*, **131**(1): 54–64.

Marti P, Alvarez M, Kaufmann W and Sigrist V (1998), "Tension Chord Model for Structural Concrete," *Structural Engineering International*, **8**(4): 287–298.

Mazzoni S, McKenna F, Scott MH, Fenves GL and Jeremic B (2006), *Open System for Earthquake Engineering Simulation Opensees Command Language Manual*, Pacific Earthquake Engineering Research Center, University of California at Berkeley, Berkeley, CA.

Mohd Yassin MH (1994), "Nonlinear Analysis of Prestressed Concrete Structures under Monotonic and Cyclic Loads," *PhD Dissertation*, University of California at Berkeley, Berkeley, CA.

Monti G and Spacone E (2000), "Reinforced Concrete Fiber Beam Element with Bond-Slip," *Journal of Structural Engineering*, **126**: 654–661.

Palermo D and Vecchio FJ (2003), "Compression Field Modeling of Reinforced Concrete Subjected to Reversusd Loading: Formulation," *ACI Structural Journal*, **100**(5): 616–625.

Palermo D and Vecchio FJ (2007), "Simulation of

Cyclically Loaded Concrete Structures Based on the Finite-Element Method," *Journal of Structural Engineering*, **133**(5): 728–738.

Pan Wenhao, Tao Muxuan and Nie Jianguo (2017), "Fiber Beam-Column Element Model Considering Reinforcement Anchorage Slip in the Footing," *Bulletin of Earthquake Engineering*, **15**(3): 991–1018.

Rehm G (1961), "Über die Grundlagen des Verbundes zwischen Stahl und Beton," Deutscher Ausschuss für Stahlbeton, 138, Ernst Berlin, Germany. (in Germany)

Scott HD, Park R and Priestly MJN (1982), "Stress-Strain Behavior of Concrete Confined by Overlapping Hoops at Low and High Strain Rates," *Journal of the American Concrete Institute*, **79**(1): 13–27.

Seckin M (1981), "Hysteretic Behavior of Cast-in-Place Exterior Beam-Column Sub Assemblies," *PhD Thesis*, University of Toronto, Toronto, ON, Canada.

Sezen H and Setzler EJ (2008), "Reinforcement Slip in Reinforced Concrete Columns," *ACI Structural Journal*, **105**(3): 280–289.

Shima H, Kanakubo T, Uchida Y and Watanabe K (2011), "Technical Committee on Bond Models and Their Applications for Numerical Analyses," *Committee Rep. JCI-TC092A*, Japanese Concrete Institute, Tokyo, 25–48.

So M, Harmon TG, Yun GJ and Dyke S (2009), "Inclusion of Smeared Cyclic Bond-Slip Behavior in Two-Dimensional Membrane Elements," *ACI Structural Journal*, **106**(4): 466–475.

So M, Harmon TG and Dyke S (2010), "FEA Implementation of Smeared Cyclic Bond Slip-Based Two-Dimensional Membrane Model," *ACI Structural Journal*, **107**(1): 92–100.

Stevens NJ, Uzumeri SM, Collins MP and Will GT (1991), "Constitutive Model for Reinforced Concrete Finite Element Analysis," *ACI Structural Journal*, **88**(1): 49–59.

Vecchio FJ and Collins MP (1986), "The Modified Compression-Field Theory for Reinforced Concrete Elements Subjected to Shear," *ACI Structural Journal*, **83**(2): 219–231.

Yokoo Y and Nakamura T (1977), "Nonstationary Hysterectic Uniaxial Stress-Strain Relations of a Steel Bar," *Transactions of the Architectural Institute of Japan*, Tokyo, Japan, **260**: 71–80.

Zhang Xuhui, Wang Lei, Zhang Jianren and Liu Yongming (2016), "Model for Flexural Strength Calculation of Corroded RC Beams Considering Bond-Slip Behavior," *Journal of Engineering Mechanics*, 04016038.